JACS
JOURNAL OF THE AMERICAN CHEMICAL SOCIETY
Article
pubs.acs.org/JACS

Photophysics of Singlet and Triplet Intraligand Excited States in [ReCl(CO)$_3$(1-(2-pyridyl)-imidazo[1,5-α]pyridine)] Complexes

Ana María Blanco-Rodríguez,[†] Hana Kvapilová,[‡] Jan Sýkora,[‡] Michael Towrie,[§] Carlo Nervi,[∥] Giorgio Volpi,[∥] Stanislav Záliš,*[,‡] and Antonín Vlček, Jr.*[,†,‡]

[†]School of Biological and Chemical Sciences, Queen Mary University of London, Mile End Road, London E1 4NS, United Kingdom

[‡]J. Heyrovský Institute of Physical Chemistry, Academy of Sciences of the Czech Republic, Dolejškova 3, CZ-182 23 Prague, Czech Republic

[§]Central Laser Facility, STFC, , Rutherford Appleton Laboratory, Harwell Oxford Science and Innovation Campus, Didcot, Oxfordshire OX11 0QX, United Kingdom

[∥]Department of Chemistry and NIS, University of Turin, Via P. Giuria 7, I-10125 Torino, Italy

Supporting Information

ABSTRACT: Excited-state characters and dynamics of [ReCl(CO)$_3$(3-R-1-(2-pyridyl)-imidazo[1,5-α]pyridine)] complexes (abbreviated **ReGV-R**, R = CH_3, Ph, $PhBu^t$, $PhCF_3$, $PhNO_2$, $PhNMe_2$) were investigated by pico- and nanosecond time-resolved infrared spectroscopy (TRIR) and excited-state DFT and TD-DFT calculations. Near UV excitation populates the lowest singlet state S_1 that undergoes picosecond intersystem crossing (ISC) to the lowest triplet T_1. Both states are initially formed hot and relax with ~20 ps lifetime. TRIR together with quantum chemical calculations reveal that S_1 is predominantly a $\pi\pi^*$ state localized at the 1-(2-pyridyl)-imidazo[1,5-α]pyridine (= impy) ligand core, with impy → $PhNO_2$ and $PhNMe_2$ → impy intraligand charge-transfer contributions in the case of **ReGV-PhNO$_2$** and **ReGV-PhNMe$_2$**, respectively. T_1 is predominantly $\pi\pi^*$(impy) in all cases. It follows that excited singlet and corresponding triplet states have to some extent different characters and structures even if originating nominally from the same preponderant one-electron excitations. ISC occurs with a solvent-independent (CH_2Cl_2, MeCN) 20−30 ps lifetime, except for **ReGV-PhNMe$_2$** (10 ps in CH_2Cl_2, 100 ps in MeCN). ISC is 200−300 times slower than in analogous complexes with low-lying MLCT states. This difference is interpreted in terms of spin−orbit interaction and characters of orbitals involved in one-electron excitations that give rise to S_1 and T_1 states. **ReGV-R** present a unique case of octahedral heavy-metal complexes where the S_1 lifetime is long enough to allow for separate spectroscopic characterization of singlet and triplet excited states. This study provides an insight into dynamics and intersystem crossing pathways of low-lying singlet and triplet excited states localized at bidentate ligands bound directly to a heavy metal atom. Rather long ^{1}IL lifetimes indicate the possibility of photonic applications of singlet excited states.

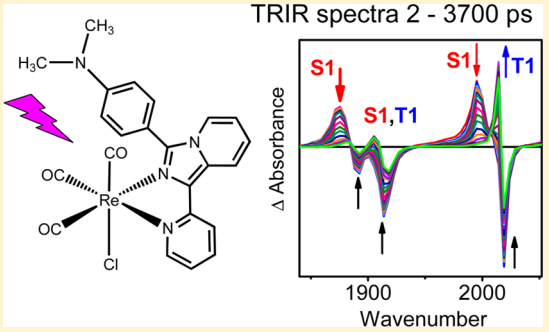

INTRODUCTION

Understanding the nature and behavior of spin-singlet and triplet excited states and factors governing their conversion dynamics (intersystem crossing, ISC) in heavy-metal complexes is an intriguing scientific problem, highly relevant to developing various photonic applications. Singlet excited states are directly excited by photon absorption, serving as excitation energy gateways, whereas triplet states of these molecules often are long-lived and emissive. Their efficient population by ISC is a necessary prerequisite for using metal complexes as luminophores in OLEDs, phosphorescence imaging of biological structures, or as photosensitizers and triggers of electron transfer reactions. Excited singlet states are usually too short-lived to have chemistry of their own or even to be detected, except by femtosecond fluorescence upconversion.[1−4] Still, they can behave differently from corresponding triplets and could play a role in light energy harvesting by undergoing ultrafast electron transfer, competitive with ISC.[5−7] Trends in ISC rates in series of structurally related metal complexes present another intriguing problem as they generally do not correlate with the spin−orbit coupling (SOC) energy. For example, ISC in Fe^{II} and Ru^{II} bipyridine complexes is comparable (≲30 fs) and slightly faster[1,8,9] than in analogous Os^{II} compounds (50−100 fs)[10] or Re^{I} carbonyl-diimines (80−150 fs),[2−4] opposite to the SOC energy increasing in the order Fe < Ru < Os. Moreover, within the [ReX(CO)$_3$(bpy)] series, the ISC rate increases in the order X = I (150 fs) < Br (130 fs) < Cl (90 fs), that is with decreasing SOC introduced by the halide ligand.[2] On the other hand, changing the bpy ligand for 1,10-phenanthroline or 4,7-

Received: December 24, 2013
Published: March 26, 2014

   dx.doi.org/10.1021/ja413098m | J. Am. Chem. Soc. 2014, 136, 5963−5973

dimethyl-1,10-phenanthroline has almost no effect.[4] Recent theoretical and experimental studies indicate[11,12] that the very notion of singlet and triplet states in metal diimine complexes could be inadequate, as was recognized already in 1974 by Crosby et al.[13] Interpreting photophysics in terms of spin−orbit states instead of singlets and triplets would allow us to discuss ISC and internal conversion in a common way and focus on the role of other effects such as vibronic coupling and distribution of excited states.[11,12,14]

Rhenium(I) tricarbonyl diimine complexes are excellent systems to investigate photophysical mechanisms as well as important luminophores and sensitizers. They exhibit rich photobehavior that stems from the occurrence of different excited states whose relative energies, properties, and reactivity can be controlled by variations of the structure and/or the medium.[15−17] Complexes with lowest-lying metal-to-ligand charge transfer (MLCT) excited states were studied most and often are used as electron-transfer triggers,[18−23] photocatalysts,[24,25] as well as luminescent probes, sensors and biomolecular imaging agents.[26−28] Re^{I} complexes with lowest $\pi\pi^*$ intraligand (IL) excited states are less common, but important as DNA probes[29−31] and molecular photoswitches.[32−35] Low-lying excited states acquire a predominantly IL character in those $[ReL(CO)_3(diimine)]^n$ complexes where the diimine ligand consists of an extensively π-delocalized aromatic system, is a poor electron acceptor, and/or where the axial ligand L is a strong electron acceptor, such as CO, alkyne, or isonitrile.[17] Photophysics of low-lying IL states are virtually unknown except for DNA intercalators $[Re^{I}(pyridine)(CO)_3(R_2dppz)]^+$ (dppz = dipyrido-[3,2-*a*:2′,3′-*c*]-phenazine)[29,30,36−38] whose lowest-lying ^{3}IL states are populated alongside or via close-lying ^{3}MLCT states. Recently synthesized Re^{I} carbonyl-dipyrrinato and aza-dipyrromethene complexes present another interesting class of complexes with low-lying singlet and triplet IL states. They show strong visible absorption and weak red phosphorescence and undergo CO photosubstitution upon UV (but not vis) irradiation.[39,40]

The complexes $[ReCl(CO)_3$(3-R-1-(2-pyridyl)-imidazo[1,5-α]pyridine)] (Figure 1, further abbreviated **ReGV-R**) offer a unique opportunity to systematically investigate properties and dynamics of IL states. The chelating 1-(2-pyridyl)-imidazo[1,5-α]pyridine ligand core (abbreviated impy) is electron-rich, pushing both ^{1,3}MLCT states to higher energies, above the ^{1,3}IL states, as was demonstrated by UV−vis absorption and photoluminescence spectroscopy, together with TD-DFT calculations.[41,42] By changing the R-group, it is possible to append electron-donating (Me), -withdrawing (-Ph, -$PhCF_3$, -$PhNO_2$), or -reducing (-$PhNMe_2$) groups to the impy core (Figure 1). Using pico−nanosecond TRIR spectroscopy and excited-state DFT calculations, we have separately characterized singlet and triplet IL excited states and determined the ISC rate, which was found to be 200−300 times slower than in analogous complexes with MLCT lowest excited states.

EXPERIMENTAL SECTION

Materials. The investigated complexes (Figure 1) were synthesized and characterized using literature methods.[41,42] Samples for TRIR measurements were prepared in MeCN and CH_2Cl_2 (DCM) of spectroscopic quality (Sigma-Aldrich), under air, unless stated otherwise. Fluorescence spectra were measured from solutions made of degassed MeCN (Aldrich SureSeal) in a controlled atmosphere (0.3 ppm of O_2) glovebox (Jacomex).

Time-Resolved IR Spectroscopy, TRIR. TRIR measurements in the ν(CO) spectral region were carried out using the PIRATE instrument at the STFC Rutherford Appleton Laboratory.[43−45] In the 0−3700 ps time domain, the sample solution was excited (pumped) at 400 nm, using frequency-doubled pulses from a titanium sapphire laser of ∼150 fs duration (fwhm) and ∼3 μJ energy, focused at an area ∼200 μm in diameter. TRIR spectra were probed with spectrally broad IR pulses (∼150 fs, width ∼200 cm^{-1}) obtained by difference-frequency generation from the same titanium sapphire laser and focused to a ∼100 μm diameter in the sample. In the nanosecond range, sample excitation was performed with 355 nm, ∼0.7 ns fwhm, ∼3 μJ laser pulses generated by an actively Q-switched AOT-YVO-20QSP/MOPA Nd:Vanadate diode-pumped microlaser, that was electronically synchronized with the femtosecond probe system with less than 400 ps jitter.[46] The 400 or 355 nm pump beams were set at the magic angle to the probe. Changes in infrared absorption at various pump−probe time delays were recorded by normalizing the outputs from a pair of 64-element HgCdTe (MCT) infrared linear array detectors on a shot-by-shot basis at 1 kHz. Data were collected in pump-on/pump-off pairs to minimize the effect of long-term drift in the laser intensity. Spectra of **ReGV-Ph** and **ReGV-PhBu^t** were also measured on the ULTRA instrument[47] that uses ∼50 fs pulses of ∼1 μJ energy at a 10 kHz repetition rate generated by titanium sapphire laser-based regenerative amplifier (Thales), focused to an area of ∼100 μm diameter. Probe pulses cover about 400 cm^{-1} range. Spectra at given time delays in the 0−2000 ps range were recorded on two 128 element HgCdTe detectors (Infrared Associates). For both setups, the sample solutions were flowed through a 0.1 mm path length cell with 2 mm CaF_2 windows that was at the same time scanned−rastered across the irradiated area in two dimensions to prevent laser heating and decomposition of the sample. FTIR spectra were measured before and after TRIR experiments to check the sample stability. Spectral and kinetics fitting procedures were performed using MicroCal Origin 7.1.

Photoluminescence Spectra and Lifetimes. Stationary emission spectra were obtained on the Fluorolog-3 instrument (model

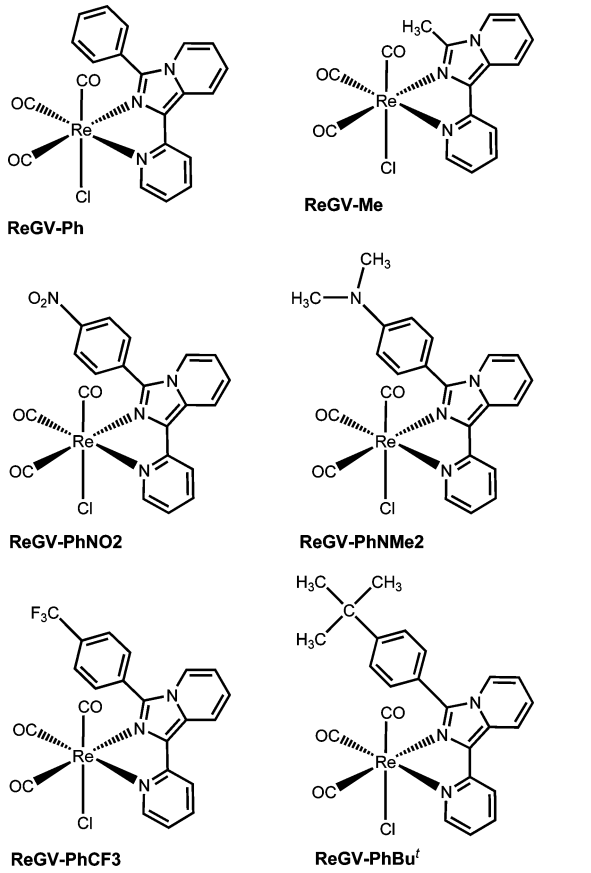

Figure 1. Schematic structures and abbreviations of the investigated **ReGV-R** complexes.

dx.doi.org/10.1021/ja413098m | J. Am. Chem. Soc. 2014, 136, 5963−5973

FL3-11; HORIBA Jobin Yvon). Emission decay lifetimes were measured at 560 nm on an IBH 5000 U SPC instrument equipped with a cooled Hamamatsu R3809U-50 microchannel plate photomultiplier. Samples were excited at 373 nm with an IBH NanoLED-11 diode laser (80 ps fwhm).

DFT Calculations. Electronic structures were calculated by density functional theory (DFT) method using the Gaussian 09[48] and ADF2013[49,50] program packages. DFT calculations employed Perdew, Burke, Ernzerhof[51,52] PBE0 or M05-2X[53] hybrid functionals. For H, C, N, and O atoms, either polarized triple-ζ basis sets 6-311g(d)[54] were used. Rhenium orbitals were described with quasi-relativistic effective core pseudopotentials and a corresponding optimized set of basis functions.[55,56] Geometry optimizations were followed by vibrational analyses in order to characterize stationary states. The solvent (dichloromethane or acetonitrile) was described by the polarizable continuum model (PCM)[57] for the ground- and excited states. Low-lying excitation energies were calculated by time-dependent DFT (TD-DFT) at the optimized geometries.

Spin orbit TD-DFT calculations were done with ADF. Slater-type orbitals (STO) basis sets of triple-ζ quality with two polarization functions for Re and double-ζ quality with one polarization function for remaining atoms were employed. PBE0 hybrid functional[51,52] together with the scalar relativistic (SR) zero-order regular approximation (ZORA)[58] and the COSMO model[59] for the solvent effect corrections. Several lowest excited states have also been calculated by the perturbational approach[60] or by the relativistic two-component zeroth-order regular approximation in TDDFT method.[61] The difference density plots were drawn using the GaussView software.

RESULTS AND DISCUSSION

Structures and UV–Vis and IR Absorption Spectra. The investigated complexes are shown in Figure 1. Previous crystallographic studies revealed that the ligand plane is slightly tilted relative to the $Re(CO)_2$ equatorial plane and the phenyl group is rotated with respect to the rest of the ligand by 55–60°.[41,42] These structural features are well reproduced by previous as well as present DFT calculations. IR spectra (Figure S1 in the SI) in the region of C≡O stretching vibrations, ν(CO), are typical for *fac*-tricarbonyls of a C_s skeletal symmetry, consisting of a sharp band at 2021–2023 cm^{-1} and a weaker doublet with maxima at 1913–1919 and 1888–1894 cm^{-1}, attributed[15,62] to totally symmetric in-phase stretching of all three CO ligands (A′(1)), antisymmetric stretching of the two equatorial COs (A″), and out-of-phase totally symmetric CO stretching vibration (A′(2)), respectively. This assignment is supported by the present DFT vibrational analysis that also indicates a very small admixture of the axial CO stretch to the A″ mode, caused by the lack of symmetry. The lowest electronic absorption band of **ReGV-R** complexes occurs at about 380 nm as an intense broad structured feature (Figure 2) that consists of several intraligand (IL) and MLCT transitions (Tables S1–S3 in the SI).[41,42]

Time-Resolved Spectroscopy. Ultrafast excited-state dynamics were investigated by time-resolved IR (TRIR) spectroscopy in the ν(CO) region measured at selected time delays after 400 nm laser pulse excitation that populates[41,42] an intraligand (^{1}IL) excited state. Spectra in the nanosecond range were measured upon 355 nm irradiation into the high-energy side of the lowest electronic absorption band. TRIR spectra of the **ReGV-PhR** and **ReGV-CH$_3$** complexes covering the ν(CO) region are presented in Figure 3; the **ReGV-PhBu^t** spectrum is shown in Figure S2 in the SI. The high-energy part of the spectra was measured also with a high resolution of ∼2 cm^{-1} per point (Figure 4). All investigated complexes exhibit a

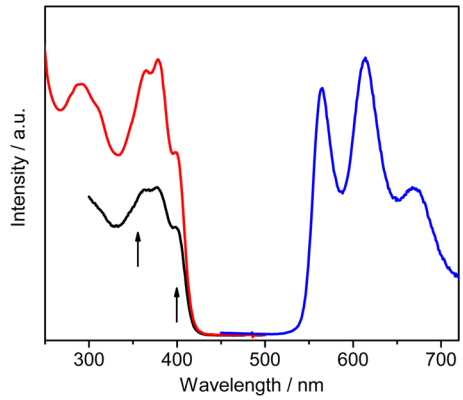

Figure 2. Electronic absorption (red), emission (blue, excited at 380 nm) and excitation (black, detected at 564 nm) spectra of **ReGV-Ph** in MeCN. The arrows show the laser excitation wavelengths of 355 and 400 nm used in the TRIR experiments. Absorption and emission spectra of other **ReGV-R** complexes are similar and shown in the literature.[41,42]

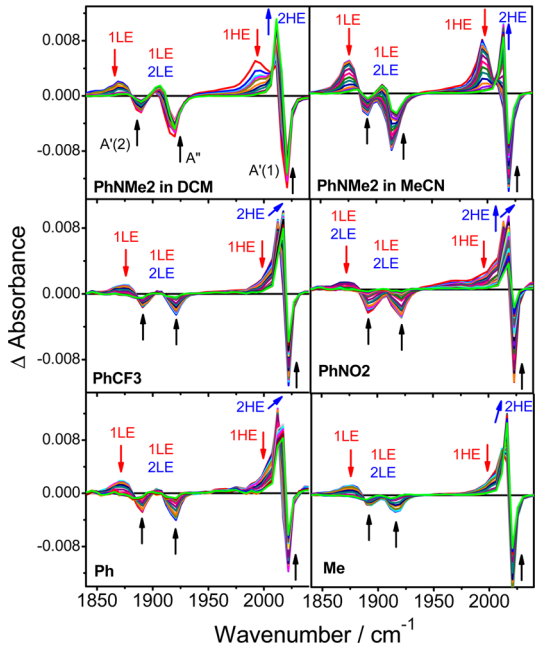

Figure 3. TRIR spectra of **ReGV-PhR** and **ReGV-Me** in DCM (except top right) measured in the 2–3700 ps interval after ∼150 fs, 400 nm excitation. Arrows indicate the temporal evolution of the spectral features: red and blue for the primary and secondary patterns, respectively; black for the bleaches. Spectral resolution: 4–5 cm^{-1} per point. The first and last spectra are shown in red and green, respectively. The intensity decrease of the 2HE feature at later times is only apparent because of its shift into the A′(1) bleach region. The 1LE and 2LE features overlap strongly with each other as well with A′(2) and A″ bleaches. (**ReGV-PhBu^t** spectra are shown in Figure S2.)

qualitatively similar behavior that can be summarized as follows:

(1) TRIR spectral evolution can be understood in terms of negative bleach bands due to depleted ground-state absorption and two time-dependent overlapping transient spectral patterns. The primary pattern (1) emerges within the instrument time resolution (<1 ps) and converts on a tens-of-picosecond time scale into the secondary pattern (2) that then slowly decays to the ground state. Each pattern consists of

dx.doi.org/10.1021/ja413098m | J. Am. Chem. Soc. 2014, 136, 5963–5973

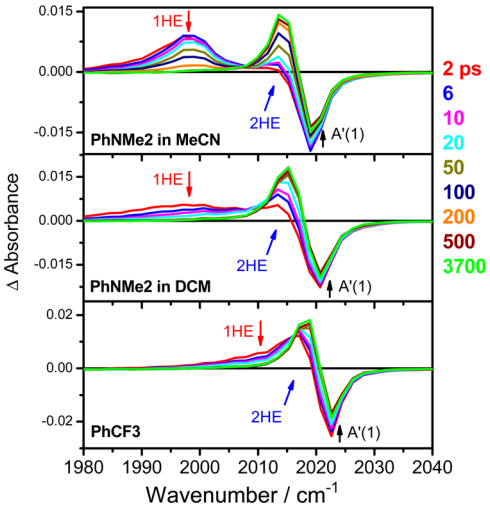

Figure 4. High-resolution TRIR spectra of selected **ReGV-PhR** complexes measured in the 2−3700 ps interval after 400 nm, ∼150 fs excitation. Arrows indicate temporal evolution of the spectral features: red and blue arrows for the primary and secondary patterns, black for the bleaches. Resolution 1.8−1.9 cm^{-1} per point. TRIR spectra of **ReGV-PhBu^t**, **-PhCH$_3$**, and **-PhNO$_2$** are very similar to those of **ReGV-PhCF$_3$**.

high-energy (HE) and low-energy (LE) spectral features which partly overlap with each other and with the bleach bands (Figures 3 and S2 in the SI). The presence of distinct 1HE and 2HE bands is obvious in the case of **ReGV-PhNMe$_2$** whereas 1HE appears as a shoulder for other complexes. In these cases, the 1HE and 2HE features were distinguished by analyzing the high-resolution spectra by shape fitting to multiple Lorentzians and attributed to two different transient species. Typical fits are shown in Figures S3−S6 in the SI. Changing the solvent (DCM, MeCN) causes small shifts of **ReGV-PhNMe$_2$** transient bands (Figures 3, 4, S3 in the SI) but has virtually no effect on the TRIR spectra of **ReGV-Ph** and **ReGV-PhBu^t** (Figures 3, S7 in the SI). None of the complexes showed any transient absorption above the A′(1) bleach (>2022 cm^{-1}), excluding population of MLCT states.

(2) The primary TRIR pattern consists of two broad features between 1860 and 1920 cm^{-1} (1LE) and in the 1995−2011 cm^{-1} range (1HE). The 1HE feature is best developed for **ReGV-PhNMe$_2$**, where it appears as a broad distinct band at 1998 cm^{-1} in MeCN (2000 cm^{-1} in DCM), shifted ∼20 cm^{-1} below the ground-state A′(1) band. For all other complexes, 1HE occurs as a broad shoulder that overlaps with the 2HE band of the secondary spectral pattern. Lorentzian shape fitting (Figures S3−S6 in the SI) places the 1HE maximum at 2006−2008 cm^{-1} in DCM, regardless of the particular ligand substituent.

(3) The secondary spectral pattern shows a broad 2LE absorption in the 1880−1920 cm^{-1} range and a sharp 2HE band at 2014−2019 cm^{-1}, depending on the particular complex. (For **ReGV-PhNMe$_2$**: 2014−2015 cm^{-1} in both DCM and MeCN, measured at time delays >200 ps.) The 2HE maximum typically lies 4−5 cm^{-1} below the A′(1) bleach for all **ReGV-PhR** and 6−7 cm^{-1} for **ReGV-Me**. Neither the shape nor position of the 2LE feature can be determined because of an extensive overlap with 1LE and the ground-state bleach. The 2LE feature lies at slightly higher wavenumbers than 1LE for all complexes except **ReGV-PhNO$_2$**, where 2LE lies slightly lower than (or comparable with) 1LE.

(4) Temporal evolution of the IR spectra combines conversion of the primary to the secondary pattern with small dynamic shifts of all bands to higher wavenumbers and their narrowing. Whereas the pattern conversion manifests a structural change of the photogenerated transient species, the continuous band shift/narrowing is due[45,63,64] to vibrational cooling and solvent relaxation. Kinetics analysis is complicated by similar time scales of all these processes and overlap between different spectral features. (For example, the bleach recovery and the 2HE decay on the ps time scale are only apparent, caused by the positive transient spectral features moving more into the bleach regions of negative absorptions, instead of transient decay to the ground state.)

The spectral pattern conversion is best observable in the case of **ReGV-PhNMe$_2$**, where the IR bands are narrower and well separated. The conversion is manifested by an isobestic 1HE decay accompanied by a 2HE rise. The 1HE and 2HE band areas decrease and increase, respectively, with a common lifetime of ∼10 ps in DCM (1HE: 9.1 ± 0.7 ps; 2HE: 10.0 ± 0.4 ps) and ∼100 ps in MeCN (1HE: 92 ± 5; 2HE: 102 ± 6 ps) (Figure 5). The 1LE band decays concomitantly with the

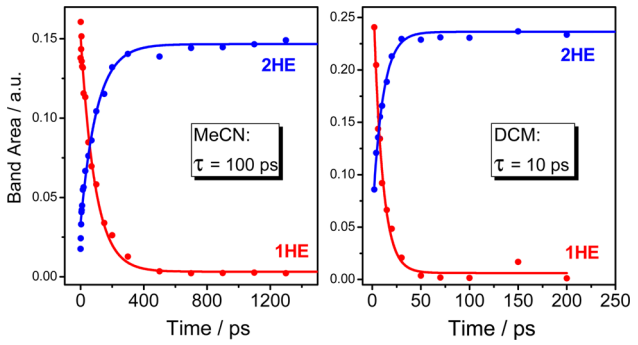

Figure 5. Time-dependence of 1HE and 2HE band areas of **ReGV-PhNMe$_2$** in MeCN (left) and DCM (right). Areas were determined by Lorentzian fitting of high-resolution TRIR spectra, Figure S3 in the SI.

1HE decay but the kinetics analysis is affected by an overlap with shifting 2LE band: 87 ± 2 ps (MeCN); 13−16 ps (DCM). Other **ReGV-PhR** and **ReGV-CH$_3$** complexes show a common behavior: A concomitant decay of the 1LE and 1HE features and 2HE rise with lifetimes in the 20−30 ps range, measured in DCM. Changing the solvent to MeCN was examined for **ReGV-Ph** and **ReGV-PhBu^t** and found to have virtually no effect on the conversion kinetics (Figure S7 in the SI). (Somewhat exceptional behavior was observed for **ReGV-PhNO$_2$**, where the 1LE/2LE feature is partly formed in <1 ps, then increases further and decays with lifetimes of 16 ± 8 ps and 31 ± 10 ps, respectively. Both 1HE and 2HE features are very broad at short time delays and overlap extensively with each other, complicating kinetics analysis. 2HE narrowing occurs with a 37 ± 2 ps lifetime.)

Dynamic 1HE and 2HE band shifts and narrowing were quantified for **ReGV-PhNMe$_2$** using Lorentzian fits (Figure 6). The 1HE band in MeCN undergoes ∼2 cm^{-1} upshift in 15 ps and ∼35% narrowing completed in the first 10 ps. The 2HE band shifts by +0.8 cm^{-1} with a 21 ± 1 ps lifetime. In DCM, 2HE shifts by 1.5 cm^{-1}, with a 20 ± 1 ps lifetime and narrows by ∼15% with a 30−40 ps lifetime. Similar 2HE shifts and narrowing were observed for other complexes, although the analysis is prevented by more extensive spectral overlaps.

dx.doi.org/10.1021/ja413098m | J. Am. Chem. Soc. 2014, 136, 5963−5973

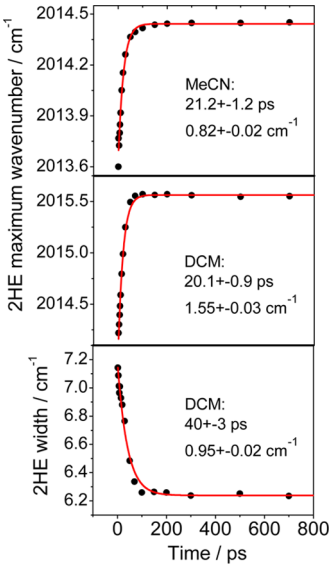

Figure 6. Time-dependence of the maximum wavenumber (top, middle) and the width (bottom) of the 2HE band of **ReGV-PhNMe$_2$**. Band maxima and widths (fwhm) were determined by Lorentzian shape-fitting (Figure S3 in the SI), and their time dependences were fitted as single-exponential functions. Lifetimes and magnitudes of the band shift/narrowing are shown in the insets.

(5) On the ns time scale (Figure 7), the 2HE and 2LE features and the bleach bands decay with a common lifetime:

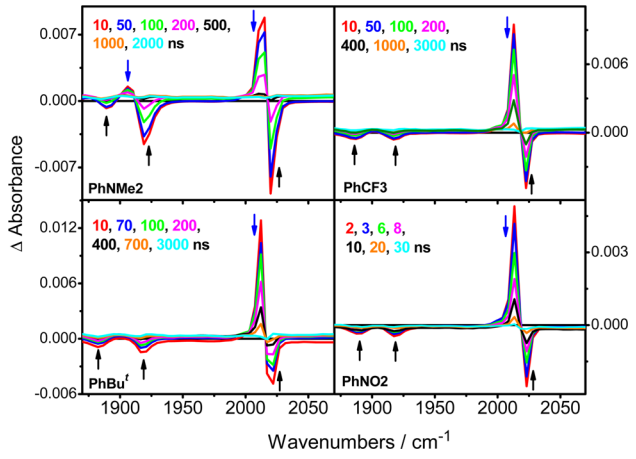

Figure 7. Nanosecond TRIR spectra of selected **ReGV-R** complexes measured in DCM at several time delays after ~0.7 ns, 355 nm excitation. Resolution: 4–5 cm^{-1}.

250 ± 17 (**ReGV-PhBu^t**, DCM), 143 ± 2 (**ReGV-PhBu^t**, MeCN), 270 ± 30 (**ReGV-PhCF$_3$**, DCM), 144 ± 2 (**ReGV-Ph**, MeCN), and 153 ± 15 ns (**ReGV-PhNMe$_2$**, DCM), measured in aerated solutions. Much faster decay of 7 ± 0.6 ns was observed for **ReGV-PhNO$_2$** in DCM. Nanosecond TRIR spectra of **ReGV-PhBu^t** in CD_3CN measured in the fingerprint region (Figure S8 in the SI) show a series of bleach- and down-shifted transient bands due to **GV-PhBu^t** ligand vibrations. All these spectral features decay together without any shifts, showing that the secondary transient does not undergo any nanosecond structural changes. The exceptionally fast decay observed for **ReGV-PhNO$_2$** is typical for metal complexes with nitro-substituted ligands, presumably due to strong coupling between the $-NO_2$ group and solvent vibrational modes.[65]

(6) All the investigated complexes except **ReGV-PhNMe$_2$** were reported to show structured long-lived phosphorescence in deaerated solutions.[41,42] Herein, we have revisited the photoluminescence of **ReGV-Ph** in MeCN (Figure 2) and determined the vibrational progression of 1376 cm^{-1}. The emission intensity in air-saturated solution decays with a 157 ± 10 ns lifetime, which is comparable with the TRIR 2HE lifetime of 144 ± 2 ns. Comparison with the lifetime measured in a degassed solution (29–37 μs) allows us to estimate the bimolecular rate constant of oxygen quenching as 3×10^9 M^{-1} s^{-1} (assuming[66] the O_2 concentration in air-saturated MeCN of 2.42×10^{-3} M). The excitation spectrum matches the absorption spectrum (Figure 2), confirming that the emitting state is populated with equal efficiency at both excitation wavelengths used in the TRIR experiments, 355 and 400 nm.

Nature of the TRIR Transients. All investigated **ReGV-R** complexes show common photophysical behavior, whereby optical excitation produces a picosecond-lived transient species that undergoes conversion into the secondary transient ultimately decaying into the ground state. The secondary species can be identified with the lowest triplet state T_1 because of its emission, long lifetime, fast oxygen quenching, and direct decay to the ground state. Conversion of the primary to the secondary species is clearly manifested in TRIR spectra by the 1HE decay accompanied by the 2HE rise and by similar changes in the LE region. It can correspond either to a conformational change (restructuring) of the T_1 state or to a nonradiative transition from a higher excited state. Given the rather rigid molecular structures of the $ReCl(CO)_3$(impy) core of the investigated complexes, conformational changes can involve rotation of the -PhR group relative to the impy plane, rotation of the $-NO_2$ group in **ReGV-PhNO$_2$**, or $-NMe_2$ rotation in **ReGV-PhNMe$_2$**. However, involvement of such rotational motions is excluded by the common spectral and dynamic characteristics of the primary and secondary spectral patterns observed for all investigated complexes, including those with a nonplanar substituent R (**ReGV-Ph**, **ReGV-PhBu^t**, **ReGV-PhCF$_3$**) and **ReGV-CH$_3$** with no pendant aromatic group. These considerations thus leave a higher excited state as the most likely assignment of the primary transient.

All ν(CO) features in both TRIR spectral patterns are shifted to lower wavenumbers from the corresponding ground-state values indicating increased Re → CO π back-donation and excluding any involvement of MLCT states. Such downshifts suggest either IL,[36−38] sigma-bond-to-ligand charge transfer (SBLCT),[67] or ligand-to-ligand charge transfer (LLCT)[68] excited states, or a ligand-localized reduction.[18−20,38,69] SBLCT and LLCT states do not occur at low energies in rhenium carbonyl diimines with chloride as the axial ligand.[17,70] GV-R ligand reduction is out of question because of very negative redox potentials (less than −2 V vs Fc^+/Fc),[41] and an absence of a reducing group, with the exception of **ReGV-PhNMe$_2$** that, however, behaves similarly to complexes containing electron-withdrawing (-PhCF$_3$) or oxidizing (-PhNO$_2$) substituents. Hence, both the primary and secondary excited states can be assigned as IL states. A slightly larger ν(CO) down-shift observed for the primary IR pattern of **ReGV-PhNMe$_2$** indicates a more extensive intraligand electron density redistribution toward the impy part of the ligand than in other **ReGV-R** complexes, likely due to the electron-donating character of the NMe_2 group. For the secondary state (T_1), the IL assignment is further supported by the characteristic structured emission and microsecond lifetimes

dx.doi.org/10.1021/ja413098m | J. Am. Chem. Soc. 2014, 136, 5963−5973

that are much longer than those[12,17,71] of analogous complexes with a ^{3}MLCT lowest excited state (usually tens of nanoseconds).

More detailed characterization of excited states involved in **ReGV-R** photophysics emerges from excited-state DFT and TD-DFT calculations that were performed on **ReGV-Ph**, **ReGV-PhNO$_2$**, and **ReGV-PhNMe$_2$**. Electron density redistribution upon the lowest transition to the S_1 singlet excited state is shown in Figure 8 and summarized in Table S4 in the SI. It follows that the S_1 transition involves $\pi \rightarrow \pi^*$ excitation of the impy part of the **GV** ligand that is combined with a $PhNMe_2$ → impy and impy → $PhNO_2$ intraligand charge transfer in the case of **ReGV-PhNMe$_2$** and **ReGV-PhNO$_2$**, respectively. Electron density on N-donor atoms and (less) on equatorial CO ligands increases in each case, accompanied by a small electron depopulation of a Re 5dπ orbital, reflecting increasing Re → CO π back-donation.

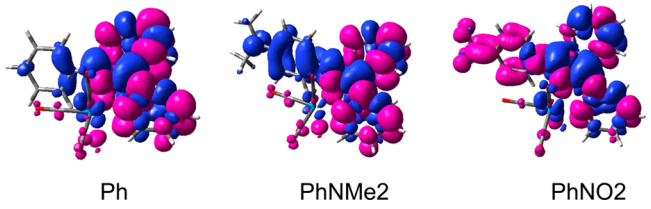

Figure 8. Electron density differences between the S_1 excited states of **ReGV-Ph**, **ReGV-PhNMe$_2$**, and **ReGV-PhNO$_2$** and the corresponding ground states. Regions of depleted and increased electron density are shown in blue and red, respectively. (TD-DFT calculation at optimized ground-state geometries, M052x, 6-31g(d), PCM for CH_2Cl_2.)

Excited-state energy diagrams (Figure 9) indicate the electronic states that could participate in the observed photophysics. At the ground-state geometry, there are several triplet states lying between the optically populated S_1 and the ground state: T_1 and T_2 for **ReGV-Ph**, T_1–T_3 for **ReGV-PhNMe$_2$**, and T_1–T_5 for **ReGV-PhNO$_2$**. The S_1 state is strongly stabilized in energy upon relaxation. Structurally optimized S_1 is separated from the ground state only by the lowest triplet T_1 in the cases of **ReGV-Ph** and **ReGV-PhNMe$_2$**, and by T_1, T_2, and T_3 for **ReGV-PhNO$_2$**, suggesting the $S_1 \rightarrow T_1$ intersystem crossing (ISC) to be the most likely mechanism responsible for the conversion observed in the TRIR spectra.

This interpretation is fully supported by the TD-DFT characterization of the S_1 and T_1 excited states whose calculated ν(CO) IR spectra match well the experimental primary and secondary ν(CO) spectral patterns, respectively. Figures 10 and S10 in the SI show that calculated IR spectra of the structurally optimized S_1 and T_1 states of **ReGV-PhNMe$_2$** and **ReGV-Ph** reproduce the conversion of the 1HE band to the higher-lying 2HE band and the small shift of the LE features to higher wavenumbers upon the $S_1 \rightarrow T_1$ ISC. The match between the calculated and experimental S_1 spectra of **ReGV-PhNO$_2$** (Figure S11 in the SI) is not as good as for the other two complexes, likely due to extensive relaxation-induced shifts and/or involvement of an intermediate state (T_2 or T_3) in the ISC that affects experimental spectra. The occurrence of such processes was indicated experimentally by the rise and decay of the 1LE+2HE feature and the large ~30 ps dynamic narrowing of both HE features, which are discussed above. In fact, the state diagram (Figure 9, right) supports the possibility that the ISC in this complex could occur via T_2 and T_3 higher excited states. Still, the calculated **ReGV-PhNO2** spectra correctly predict the T_1 2LE band occurring at slightly lower wave-

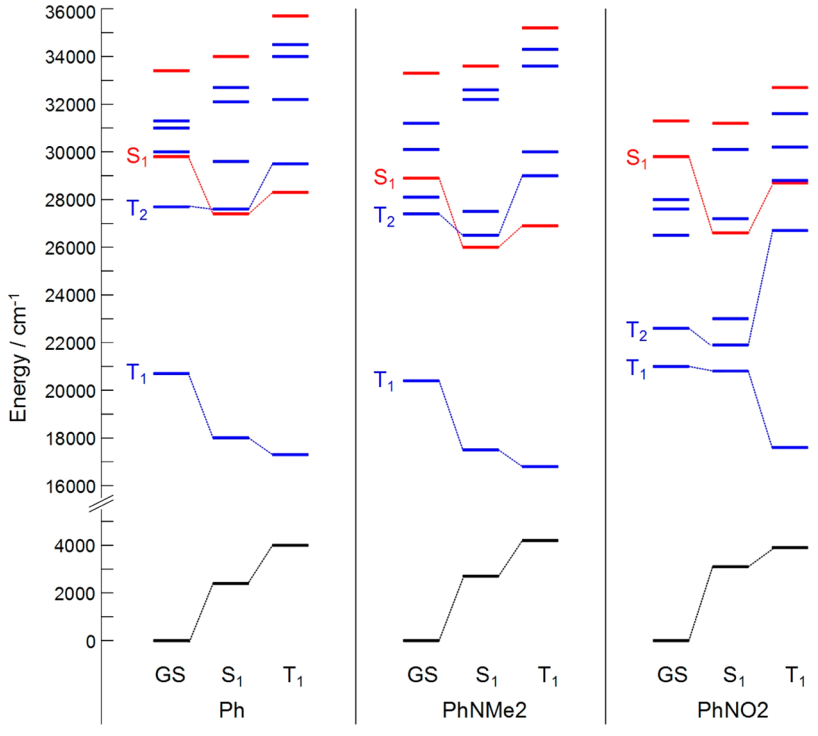

Figure 9. State energy diagram of **ReGV-Ph**, **ReGV-PhNMe$_2$**, and **ReGV-PhNO$_2$** in CH_2Cl_2. Electronic states calculated at optimized ground-state, S_1, and T_1 geometries are shown for each complex. Black: ground state; blue: triplet states; red: excited singlet states. (TD-DFT, M052x, 6-31g(d), PCM for CH_2Cl_2).

dx.doi.org/10.1021/ja413098m | J. Am. Chem. Soc. 2014, 136, 5963–5973

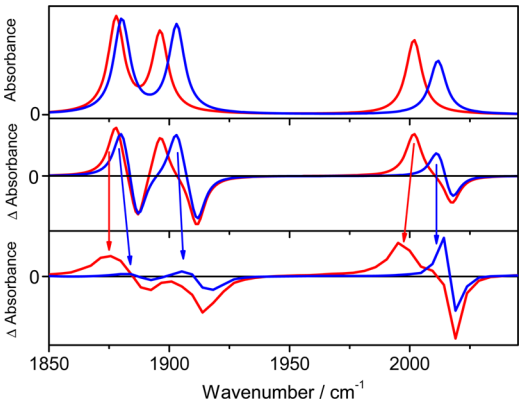

Figure 10. Calculated and experimental excited-state IR spectra of **ReGV-PhNMe$_2$** in MeCN. Top: calculated spectra of S_1 at the optimized S_1 geometry (red) and of T_1 at the optimized T_1 geometry (blue). Middle: calculated difference IR spectra of S_1 (red) and T_1 (blue) minus the ground-state spectrum calculated at the optimized ground-state geometry. Bottom: experimental TRIR spectra measured at 2 ps (red) and 3000 ps (blue). The red spectrum corresponds to a hot state and therefore is slightly broadened and shifted to lower wavenumbers. The calculated and experimental 1HE and 2HE wavenumbers match with an accuracy of 4 and 2 cm^{-1}, respectively: The 1HE band (S1 state) was calculated at 2002 cm^{-1} vs the experimental value of 1998 cm^{-1} (determined by shape-fitting of high-resolution spectra). For 2HE, the calculated and experimental values are 2012 and 2014 cm^{-1}, respectively. Calculated and experimental 1LE wavenumbers are 1878 and 1874 cm^{-1}, respectively. Calculation: TD-DFT, 6-31g(d), M052X, PCM for MeCN, scaling factor 0.940.

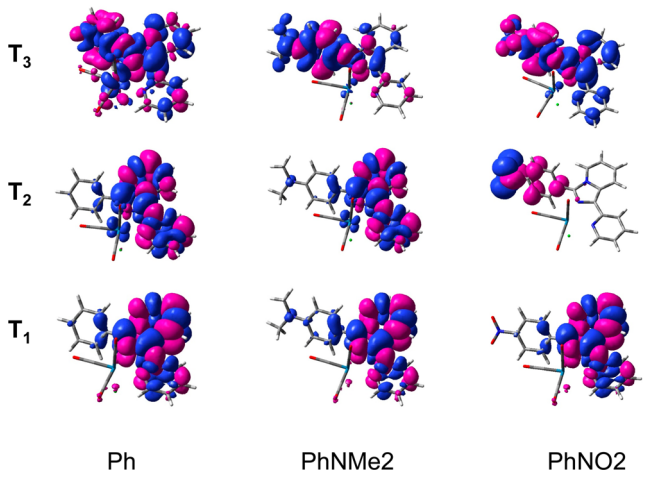

Figure 11. Electron density differences between the three lowest triplet states of **ReGV-Ph**, **ReGV-PhNMe$_2$**, and **ReGV-PhNO$_2$** and the corresponding ground states. Regions of depleted and increased electron density are shown in blue and red, respectively. (TD-DFT calculation at optimized ground-state geometries, M052x, 6-31g(d), PCM for CH_2Cl_2.)

numbers than the S_1 1LE feature, in contrast to other complexes.

The relaxed S_1 state of **ReGV-Ph** and **ReGV-PhNMe$_2$** is calculated to have a predominantly impy-localized $\pi\pi^*$ intraligand character combined with a small increase of Re → CO π donation (Table S4 in the SI). This conclusion can be extended to all other investigated complexes, except **ReGV-PhNO$_2$** whose relaxed S_1 state also is predominantly intraligand impy-localized $\pi\pi^*$, but accompanied by a limited Re → GV-PhNO$_2$ charge transfer (MLCT), leaving the electron density on CO ligands intact. The T_1 state of all three complexes was calculated to be an impy-localized $\pi\pi^*$ ^{3}IL, (Figure 9, Table S5 in the SI). This conclusion is confirmed for relaxed T_1 by spin-density distributions calculated at optimized T_1 geometries (Figure S9, Table S5 in the SI). The larger involvement of the Re(CO)$_3$ moiety in S_1 than T_1 accounts for the fact that the S_1 ν(CO) bands of the primary TRIR pattern occur at lower wavenumbers than those of the secondary pattern due to T_1. The situation is different only in the case of **ReGV-PhNO$_2$**, where the Re → GV-PhNO$_2$ CT contribution present in S_1 vanishes upon ISC to T_1. Consequently, the S_1 1LE band occurs at higher wavenumbers than the T_1 2LE feature (Figure S11 in the SI).

Finally, it is possible to conclude that any involvement of the T_2 state in the ISC is very unlikely in all investigated complexes except **ReGV-PhNO$_2$**. The T_2 electron density difference maps of **ReGV-Ph** and **ReGV-PhNMe$_2$** (Figure 11) do not show any electron density increase on CO ligands while indicating MLCT Re → GV contributions (manifested by Re d-orbital depopulation and electron density increase on the ligand). This type of electron density distribution qualitatively predicts that the T_2 ν(CO) bands would lie at higher wavenumbers than those of T_1 and cannot thus account for the primary TRIR pattern. Moreover, whereas T_1 is in all cases an impy-localized $\pi\pi^*$ state, the intraligand charge distribution in higher triplets is expected to depend on the ligand substituent. However, the observation of a similar TRIR behavior was observed for complexes with oxidizable (-PhNMe$_2$), reducible (-PhNO$_2$), electron-withdrawing (-PhCF$_3$), donating (-PhBu^t), and "inert" (-Ph, -Me) groups effectively excludes the conversion between two triplet excited states of different charge distributions as a mechanism responsible for TRIR pattern conversion.

Spin−Orbit Effects. Perturbational and two-component spin−orbit DFT calculations of **ReGV-PhNMe$_2$** were carried out using pure (BP86) as well as hybrid (B3LYP) functionals in order to further examine the validity of the above interpretation and to assess SO effects on intraligand states. In all SO calculations performed, the S_1 and T_1 states identified above remain the two lowest excited states. Zero field splitting (zfs) of the T_1 state was calculated to be very small (~0.216 cm^{-1}) and comparable with experimentally determined zfs of ^{3}IL states of Rh^{III} bpy and phen complexes (0.1−0.2 cm^{-1})[72,73] or [Ir(2-phenylpyridine)$_2$(CO)(Cl)] (<1 cm^{-1}).[74] In **ReGV-PhNMe$_2$**, zfs arises from a very small (~0.2%) SO-induced admixture of higher-lying ^{1}MLCT singlet state(s), instead of the optically populated S_1. The T_1 zfs is much smaller than that calculated (133 cm^{-1})[12] or measured (90 cm^{-1})[75] for the predominantly MLCT lowest triplet state of [ReCl(CO)$_3$(bpy)], which originates from mixing with the optically excited ^{1}MLCT state. The S_1 state of **ReGV-PhNMe2** was calculated to be essentially a pure singlet using the BP86 functional that, however, strongly underestimates the transition energy. B3LYP SO calculations indicate a 23% admixture of higher triplets to S_1 and occurrence of three more SO states with predominant triplet characters at only slightly higher energies (240−400 cm^{-1}). The sensitivity of S_1 SO calculations to the functional precludes making any detailed conclusions on the S_1 spin character. However, a significant admixture of higher MLCT triplets into S_1 is very unlikely in view of the IR spectral pattern that is typical of an IL state and the match of the experimental spectrum with that calculated for spin-free S_1 (Figure 10).

Ultrafast Excited-State Dynamics. TRIR experiments reveal two kinds of picosecond dynamics of **ReGV-R**

dx.doi.org/10.1021/ja413098m | J. Am. Chem. Soc. 2014, 136, 5963−5973

complexes: (i) decay of the S_1 state into the lowest triplet T_1 manifested by the conversion of the primary TRIR spectral pattern to the secondary one, and (ii) structural/solvational relaxation of both S_1 and T_1 that is revealed by small dynamic 1HE and 2HE band shifts and narrowing.

Relaxation-induced spectral shifts occur on a time scale of ~20 ps that is slightly slower than those observed[45,63,64,76,77] in MLCT excited-state TRIR spectra of Re carbonyl-diimines in dipolar solvents (9−15 ps). The shifts are attributed[45,76,77] to cooling that includes restructuring of the first solvent shell to optimize interactions between the solvent molecules and electronically excited **ReGV-R** solute whose electron distribution over the ligand is different from that in the ground state.

The S_1 to T_1 conversion (intersystem crossing, ISC) occurs with a 20−30 ps lifetime for **ReGV-CH$_3$**, **-Ph**, **-PhBu^t**, **-PhCF$_3$**, and **-PhNO$_2$** in DCM, and about 10 ps in the case of **ReGV-PhNMe$_2$**. Changing the solvent to more polar MeCN has no effect on the ISC rate of **ReGV-Ph** and **ReGV-PhBu^t** but slows down ISC in **ReGV-PhNMe$_2$** 10-times to ~100 ps. ISC in **ReGV-R** is 200−300 times slower than in [ReCl(CO)$_3$(bpy)] and [ReCl(CO)$_3$(phen)] (85−110 fs, depending on the solvent).[2−4] This huge change in the ISC rate is attributable to two effects: different excited-state characters and different symmetry constraints. The femtosecond ISC in bpy and phen complexes involves singlet and triplet states of a predominantly MLCT character with ~50% Re 5d orbital participation in the depopulated molecular orbitals.[2,4] More importantly, the optically populated ^{1}MLCT and the lowest ^{3}MLCT states differ in the symmetry of the 5d orbital involved, and hence, ISC is accompanied by orbital rotation that compensates for the change in the spin momentum.[2] The ^{1,3}MLCT states are thus directly SO-coupled, and the ISC is allowed.[2−4] The situation is very different in the case of **ReGV-R** complexes, where both S_1 and T_1 are of an IL character, arising predominantly from HOMO → LUMO excitation (Tables S1−S3 in the SI). The molecular orbitals depopulated in S_1 and T_1 are the same, no orbital rotation occurs, and ISC is forbidden according to El Sayed's rules in the same way as $^1\pi\pi^*$ → $^3\pi\pi^*$ ISC in aromatic hydrocarbons.[78] Moreover, the Re 5d participation in S_1 and T_1 is low, originating mostly from small interconfigurational mixing between HOMO → LUMO and higher MLCT excitations. In the absence of direct S_1−T_1 SO interaction (confirmed by SO calculations), ISC is probably enabled by weaker second-order interactions of S_1 with higher-lying MLCT states. The difference in the SO coupling strength and, hence, the propensity to undergo ISC between the singlet and triplet IL states in **ReGV-R** and MLCT states in [ReCl(CO)$_3$(bpy)] also is demonstrated by the vastly different zfs magnitudes, 0.2 vs 133 cm^{-1}, see above.

The S_1 and T_1 states in **ReGV-Ph**, **-PhBu^t**, and **-PhCF$_3$** behave as $\pi\pi^*$ excited states with small Re(CO)$_3$ contributions. There are no large differences in the charge distribution between the ground states and the two excited states in question (Tables S4, S5 in the SI). Consequently, the ISC rates of **ReGV-Ph** and **ReGV-PhBu^t** are insensitive to the solvent polarity, DCM vs MeCN. On the other hand, the pronounced solvent effect on the ISC rate in **ReGV-PhNMe$_2$** likely is due to the larger intraligand charge-transfer character of S_1 than T_1 that makes their energy gap and vibronic coupling sensitive to the solvent polarity.

CONCLUDING REMARKS

ReGV-R are an unusual class of heavy metal complexes in which the lowest lying singlet as well as triplet excited states are predominantly localized at a *N*,*N*-chelating ligand that is directly coordinated to the metal atom. In this respect, **ReGV-R** differ from the other prominent class of compounds showing ligand-localized photophysics and photochemistry, namely [Pt(L$_2$)(C≡CR′)$_2$] and [Pt(terpyridine)(C≡CR′)]$^+$, where the $\pi\pi^*$ IL states are localized predominantly at a pendant aromatic group R′, such as naphthalene,[79] pyrene,[80] perylene-diimide,[81,82] or stilbene[83] (L$_2$ = 4,4′-Bu^t-bpy or diphosphine). **ReGV-R** photophysics also differ from those of DNA intercalators [Re(L)(CO)$_3$(dppz)]$^+$ whose lowest ^{3}IL state is populated on a subpicosecond time scale via MLCT states and, in some cases, occurs in a thermal equilibrium with ^{3}MLCT.[29,30,36−38]

ReGV-R present a rare case where both the optically populated excited singlet and the lowest triplet states were characterized spectroscopically. It turns out that these two states differ considerably in their respective characters, despite being nominally derived from the same preponderant one-electron excitation, *i.e.* HOMO → LUMO. This difference is most pronounced for **ReGV-NMe$_2$**, where both S_1 and T_1 are essentially $\pi\pi^*$ excited states of the impy ligand core but S_1 contains an additional PhNMe$_2$ → impy charge transfer component. The Re(CO)$_3$ electronic involvement, although small in absolute terms, is larger for S_1 than T_1. Such differences result from a different extent of interconfigurational mixing of higher one-electron excitations into S_1 and T_1. On the other hand, **ReGV-R** complexes without strongly donating (or accepting) substituents such as **ReGV-Ph** or **ReGV-CH$_3$** have both S_1 and T_1 states localized mostly at the impy part of the ligand but still with somewhat different IR spectra and, hence, electronic structures. Quadruply bonded W^{II} dimers with electron-accepting bridging ligands present another case, showing differences in singlet and triplet excited-state IR spectra that indicate a larger electron density on the ligand in the $^1\delta\pi^*$ than the $^3\delta\pi^*$ MLCT state.[84,85] In the case of 2,5-bis(*p*-arylethynyl)cyclopentadiene complexes of Rh^{III}, a larger ν(C≡C) IR shift was observed on going from the ground state to the lowest ^{3}IL state than to the corresponding excited singlet.[86]

The slow ISC between the S_1 and T_1 IL states in **ReGV-R**, as compared with MLCT states in [ReCl(CO)$_3$(bpy)] and similar complexes, is due not only to smaller Re 5d participation but mainly to different symmetry constraints which allow for a direct SO coupling between the optically populated ^{1}MLCT and the lowest ^{3}MLCT states but not between IL singlets and triplets. The relative orientation (rotation) of the depopulated orbital in the singlet and triplet is the decisive factor. Direct SO coupling between ^{1,3}MLCT states leads to a large zfs and femtosecond ISC that can be treated as a vibronic transition between two spin−orbit states.[11,12] On the other hand, the intraligand T_1 zfs is very small, and the S_1 → T_1 ISC involves second-order coupling via higher excited states. Indeed, an identical preponderant electron configuration of the S_1 and T_1 states seems to be the key factor extending excited singlet lifetimes in **Re-GV** as well as in other types of complexes and electronic states, for example: ^{1}MLCT of pseudotetrahedral complexes of Cu^I (13−16 ps)[87] and Pt^0 (3.2 ps),[88] ^{1}dσ^*pσ in d^8−d^8 dimers such as [Pt$_2$(P$_2$O$_5$H$_2$)$_4$]$^{4-}$ (3−30 ps) and [Pt$_2$(P$_2$O$_5$BF$_2$)$_4$]$^{4-}$ (1.6 ns),[89] and for IL states in Pt complexes

dx.doi.org/10.1021/ja413098m | J. Am. Chem. Soc. 2014, 136, 5963−5973

with pendant organic chromophores: $[Pt(PBu_3)_2(C{\equiv}C\text{-pyrene})_2]$ (5.4 ps);[80] $[Pt(L_2)(C{\equiv}C\text{-perylenediimide})_2]$ (2−4 ps),[81] or $[Pt(trpy)(C{\equiv}C\text{-perylenediimide})]^+$ (109 ps).[82] Surprisingly, ^{1}IL → ^{3}IL ISC in **ReGV-R** is slower than in some of the Pt complexes, despite a direct linkage of the photophysically active ligand to the Re atom.

Metal complexes with lowest triplets of a $\pi\pi^*$ intraligand character are deemed not to be good candidates for OLED luminophores because of low phosphorescence quantum yields. This is a consequence of weak SO coupling and negligible singlet admixtures into the lowest triplet state that also are manifested by very small (<1 cm^{-1}) zfs.[90−93] The present study of **ReGV-R** photophysics confirms this picture, provides a deeper insight into spin−orbit coupling pathways in metal complexes with low-lying intraligand states, and reveals rather long ^{1}IL lifetimes. Metal complexes with picosecond-lived optically populated singlet excited states could find interesting photonic applications. For example, they could be considered as active components of molecular antennas or artificial reaction centers where the absorbed light energy would be efficiently captured and utilized either by energy- or electron transfer before being partly lost by conversion to lower-lying triplets. Long singlet lifetimes also could allow for singlet fission[94] that has yet to be observed in metal complexes.

■ ASSOCIATED CONTENT

Supporting Information

Tables of DFT-calculated low-lying singlet−singlet and singlet transitions (energies, osc. strengths), table of Mulliken charges in the S_1, T_1, and the ground-state, figures of ground-state IR spectra, TRIR of **ReGV-PhBu^t** in DCM, typical Lorentzian shape-fits of TRIR spectra, TRIR spectra of **ReGV-Ph** and **ReGV-PhBu^t** in MeCN, TRIR spectra of **ReGV-PhBu^t** in CD_3CN in the fingerprint region, calculated spin density distribution in relaxed T_1 excited states, comparison of calculated and experimental excited-state IR spectra of **ReGV-Ph** and **ReGV-PhNO2**. This material is available free of charge via the Internet at http://pubs.acs.org.

■ AUTHOR INFORMATION

Corresponding Authors

zalis@jh-inst.cas.cz (S.Z.)
a.vlcek@qmul.ac.uk (A.V.)

Notes

The authors declare no competing financial interest.

■ ACKNOWLEDGMENTS

This research was supported by STFC Rutherford Appleton Laboratory (CMSD 43), QMUL, European collaboration program COST Actions CM1002 (CODECS), and CM1202 (PERSPECT-H2O), and the Czech Ministry of Education Grant LD11086. J.S. acknowledges the Czech Science Foundation (Project P208/12/G016) for supporting the fluorescence measurements. C.N. acknowledges the support of PHOTORECARB Project (San Paolo Company, Italy).

■ REFERENCES

(1) Cannizzo, A.; van Mourik, F.; Gawelda, W.; Zgrablic, G.; Bressler, C.; Chergui, M. *Angew. Chem., Int. Ed.* **2006**, *45*, 3174−3176.
(2) Cannizzo, A.; Blanco-Rodríguez, A. M.; Nahhas, A.; Šebera, J.; Záliš, S.; Vlček, A., Jr.; Chergui, M. *J. Am. Chem. Soc.* **2008**, *130*, 8967−8974.
(3) El Nahhas, A.; Cannizzo, A.; van Mourik, F.; Blanco-Rodríguez, A. M.; Záliš, S.; Vlček, A., Jr.; Chergui, M. *J. Phys. Chem. A* **2010**, *114*, 6361−6369.
(4) El Nahhas, A.; Consani, C.; Blanco-Rodríguez, A. M.; Lancaster, K. M.; Braem, O.; Cannizzo, A.; Towrie, M.; Clark, I. P.; Záliš, S.; Chergui, M.; Vlček, A., Jr. *Inorg. Chem.* **2011**, *50*, 2932−2943.
(5) Kallioinen, J.; Benkö, G.; Sundström, V.; Korppi-Tommola, J. E. I.; Yartsev, A. P. *J. Phys. Phem. B* **2002**, *106*, 4396−4404.
(6) Benkö, G.; Kallioinen, J.; Korppi-Tommola, J. E. I.; Yartsev, A. P.; Sundström, V. *J. Am. Chem. Soc.* **2002**, *124*, 489−493.
(7) Bräm, O.; Cannizzo, A.; Chergui, M. *Phys. Chem. Chem. Phys.* **2012**, *14*, 7934−7937.
(8) Gawelda, W.; Cannizzo, A.; Pham, V.-T.; van Mourik, F.; Bressler, C.; Chergui, M. *J. Am. Chem. Soc.* **2007**, *129*, 8199−8206.
(9) Bräm, O.; Messina, F.; El-Zohry, A. M.; Cannizzo, A.; Chergui, M. *Chem. Phys.* **2012**, *393*, 51−57.
(10) Bräm, O.; Messina, F.; Baranoff, E.; Cannizzo, A.; Nazeeruddin, M. K.; Chergui, M. *J. Phys. Chem. C* **2013**, *117*, 15958−15966.
(11) Baková, R.; Chergui, M.; Daniel, C.; Vlček, A., Jr.; Záliš, S. *Coord. Chem. Rev.* **2011**, *255*, 975−989.
(12) Heydová, R.; Gindensperger, E.; Romano, R.; Sýkora, J.; Vlček, A., Jr.; Záliš, S.; Daniel, C. *J. Phys. Chem. A* **2012**, *116*, 11319−11329.
(13) Crosby, G. A.; Hipps, K. W.; Elfring, W. H. J. *J. Am. Chem. Soc.* **1974**, *96*, 629−630.
(14) Chergui, M. *Dalton Trans.* **2012**, *41*, 13022−13029.
(15) Vlček, A., Jr. *Top. Organomet. Chem.* **2010**, *29*, 73−114.
(16) Kumar, A.; Sun, S.-S.; Lees, A. J. *Top. Organomet. Chem.* **2010**, *29*, 1−35.
(17) Stufkens, D. J.; Vlček, A., Jr. *Coord. Chem. Rev.* **1998**, *177*, 127−179.
(18) Shih, C.; Museth, A. K.; Abrahamsson, M.; Blanco-Rodriguez, A. M.; Di Bilio, A. J.; Sudhamsu, J.; Crane, B. R.; Ronayne, K. L.; Towrie, M.; Vlček, A., Jr.; Richards, J. H.; Winkler, J. R.; Gray, H. B. *Science* **2008**, *320*, 1760−1762.
(19) Blanco-Rodríguez, A. M.; Di Bilio, A. J.; Shih, C.; Museth, A. K.; Clark, I. P.; Towrie, M.; Cannizzo, A.; Sudhamsu, J.; Crane, B. R.; Sýkora, J.; Winkler, J. R.; Gray, H. B.; Záliš, S.; Vlček, A., Jr. *Chem.—Eur. J.* **2011**, *17*, 5350−5361.
(20) Blanco-Rodríguez, A. M.; Towrie, M.; Sýkora, J.; Záliš, S.; Vlček, A., Jr. *Inorg. Chem.* **2011**, *50*, 6122−6134.
(21) Chen, P.; Westmoreland, T. D.; Danielson, E.; Schanze, K. S.; Anthon, D.; Neveux, P. E., Jr.; Meyer, T. J. *Inorg. Chem.* **1987**, *26*, 1116−1126.
(22) Lucia, L. A.; Wang, Y.; Nafisi, K.; Netzel, T. L.; Schanze, K. S. *J. Phys. Chem.* **1995**, *99*, 11801−11804.
(23) Liard, D. J.; Busby, M.; Farrell, I. R.; Matousek, P.; Towrie, M.; Vlček, A., Jr. *J. Phys. Chem. A* **2004**, *108*, 556−567.
(24) Takeda, H.; Koike, K.; Inoue, H.; Ishitani, O. *J. Am. Chem. Soc.* **2008**, *130*, 2023−2031.
(25) Takeda, H.; Ishitani, O. *Coord. Chem. Rev.* **2010**, *254*, 346−354.
(26) Lo, K. K.-W.; Louie, M.-W.; Zhang, K. Y. *Coord. Chem. Rev.* **2010**, *254*, 2603−2622.
(27) Lo, K. K.-W. *Top. Organomet. Chem.* **2010**, *29*, 115−158.
(28) Lo, K. K.-W.; Sze, K.-S.; Tsang, K. H.-K.; Zhu, N. *Organometallics* **2007**, *26*, 3440−3447.
(29) Olmon, E. D.; Sontz, P. A.; Blanco-Rodríguez, A. M.; Towrie, M.; Clark, I. P.; Vlček, A., Jr.; Barton, J. K. *J. Am. Chem. Soc.* **2011**, *133*, 13718−13730.
(30) Cao, Q.; Creely, C. M.; Davies, E. S.; Dyer, J.; Easun, T. L.; Grills, D. C.; McGovern, D. A.; McMaster, J.; Pitchford, J.; Smith, J. A.; Sun, X.-Z.; Kelly, J. M.; George, M. W. *Photochem. Photobiol. Sci.* **2011**, *10*, 1355−1364.
(31) Stoeffler, H. D.; Thornton, N. B.; Temkin, S. L.; Schanze, K. S. *J. Am. Chem. Soc.* **1995**, *117*, 7119−7128.
(32) Wenger, O. S.; Henling, L. M.; Day, M. W.; Winkler, J. R.; Gray, H. B. *Inorg. Chem.* **2004**, *43*, 2043−2048.
(33) Patrocinio, A. O. T.; Iha, N. Y. M. *Inorg. Chem.* **2008**, *47*, 10851−10857.

(34) Sarto Polo, A. S.; Itokazu, M. K.; Frin, K. M.; de Toledo Patrocinio, A. O.; Iha, N. Y. M. *Coord. Chem. Rev.* **2006**, *250*, 1669−1680.
(35) Ko, C.-C.; Kwok, W.-M.; Yam, V. W.-W.; Phillips, D. L. *Chem.—Eur. J.* **2006**, *12*, 5840−5848.
(36) Dyer, J.; Creely, C. M.; Penedo, J. C.; Grills, D. C.; Hudson, S.; Matousek, P.; Parker, A. W.; Towrie, M.; Kelly, J. M.; George, M. W. *Photochem. Photobiol. Sci.* **2007**, *6*, 741−748.
(37) Dyer, J.; Blau, W. J.; Coates, C. G.; Creely, C. M.; Gavey, J. D.; George, M. W.; Grills, D. C.; Hudson, S.; Kelly, J. M.; Matousek, P.; McGarvey, J. J.; McMaster, J.; Parker, A. W.; Towrie, M.; Weinstein, J. A. *Photochem. Photobiol. Sci.* **2003**, *2*, 542−554.
(38) Dattelbaum, D. M.; Omberg, K. M.; Hay, P. J.; Gebhart, N. L.; Martin, R. L.; Schoonover, J. R.; Meyer, T. J. *J. Phys. Chem. A* **2004**, *108*, 3527−3536.
(39) McLean, T. M.; Moody, J. L.; Waterland, M. R.; Telfer, S. G. *Inorg. Chem.* **2012**, *51*, 446−455.
(40) Partyka, D. V.; Deligonul, N.; Washington, M. P.; Gray, T. G. *Organometallics* **2009**, *28*, 5837−5840.
(41) Salassa, L.; Garino, C.; Albertino, A.; Volpi, G.; Nervi, C.; Gobetto, R.; Kenneth I. Hardcastle, K. I. *Organometallics* **2008**, *27*, 1427−1435.
(42) Garino, C.; Ruiu, T.; Salassa, L.; Albertino, A.; Volpi, G.; Nervi, C.; Gobetto, R.; Hardcastle, K. I. *Eur. Inorg. Chem.* **2008**, 3587−3591.
(43) Towrie, M.; Grills, D. C.; Dyer, J.; Weinstein, J. A.; Matousek, P.; Barton, R.; Bailey, P. D.; Subramaniam, N.; Kwok, W. M.; Ma, C. S.; Phillips, D.; Parker, A. W.; George, M. W. *Appl. Spectrosc.* **2003**, *57*, 367−380.
(44) Vlček, A., Jr.; Farrell, I. R.; Liard, D. J.; Matousek, P.; Towrie, M.; Parker, A. W.; Grills, D. C.; George, M. W. *J. Chem. Soc., Dalton Trans.* **2002**, 701−712.
(45) Blanco-Rodríguez, A. M.; Ronayne, K. L.; Záliš, S.; Sýkora, J.; Hof, M.; Vlček, A., Jr. *J. Phys. Chem. A* **2008**, *112*, 3506−3514.
(46) Towrie, M.; Parker, A. W.; Vlček, A., Jr.; Gabrielsson, A.; Blanco Rodriguez, A. M. *Appl. Spectrosc.* **2005**, *59*, 467−473.
(47) Greetham, G.; Burgos, P.; Cao, Q.; Clark, I. P.; Codd, P.; Farrow, R.; George, M. W.; Kogimtzis, M.; Matousek, P.; Parker, A. W.; Pollard, M.; Robinson, D.; Xin, Z.-J.; Towrie, M. *Appl. Spectrosc.* **2010**, *64*, 1311−1319.
(48) Frisch, M. J.; Trucks, G. W.; Schlegel, H. B.; Scuseria, G. E.; Robb, M. A.; Cheeseman, J. R.; Scalmani, G.; Barone, V.; Mennucci, B.; Petersson, G. A.; Nakatsuji, H.; Caricato, M.; Li, X.; Hratchian, H. P.; Izmaylov, A. F.; Bloino, J.; Zheng, G.; Sonnenberg, J. L.; Hada, M.; Ehara, M.; Toyota, K.; Fukuda, R.; Hasegawa, J.; Ishida, M.; Nakajima, T.; Honda, Y.; Kitao, O.; Nakai, H.; Vreven, T.; Montgomery, J. A., Jr.; Peralta, J. E.; Ogliaro, F.; Bearpark, M.; Heyd, J. J.; Brothers, E.; Kudin, K. N.; Staroverov, V. N.; Kobayashi, R.; Normand, J.; Raghavachari, K.; Rendell, A.; Burant, J. C.; Iyengar, S. S.; Tomasi, J.; Cossi, M.; Rega, N.; Millam, J. M.; Klene, M.; Knox, J. E.; Cross, J. B.; Bakken, V.; Adamo, C.; Jaramillo, J.; Gomperts, R.; Stratmann, R. E.; Yazyev, O.; Austin, A. J.; Cammi, R.; Pomelli, C.; Ochterski, J. W.; Martin, R. L.; Morokuma, K.; Zakrzewski, V. G.; Voth, G. A.; Salvador, P.; Dannenberg, J. J.; Dapprich, S.; Daniels, A. D.; Farkas, O.; Foresman, J. B.; Ortiz, J. V.; Cioslowski, J.; Fox, D. J. *Gaussian 09*, Revision C.01; Gaussian, Inc.: Wallingford CT, 2009.
(49) Te Velde, G.; Bickelhaupt, F. M.; van Gisbergen, S. J. A.; Fonseca Guerra, C.; Baerends, E. J.; Snijders, J. G.; Ziegler, T. *J. Comput. Chem.* **2001**, *22*, 931−967.
(50) *ADF2013.01, SCM, Theoretical Chemistry*; Vrije Universiteit: Amsterdam, The Netherlands, 2013; http://www.scm.com.
(51) Perdew, J. P.; Burke, K.; Ernzerhof, M. *Phys. Rev. Lett.* **1996**, *77*, 3865−3868.
(52) Adamo, C.; Barone, V. *J. Chem. Phys.* **1999**, *110*, 6158−6170.
(53) Zhao, Y.; Schultz, N. E.; Truhlar, D. G. *J. Chem. Theory Comput.* **2006**, *2*, 364−382.
(54) Raghavachari, K.; Binkley, J. S.; Seeger, R.; Pople, J. A. *J. Chem. Phys.* **1980**, *72*, 650−654.
(55) Andrae, D.; Häussermann, U.; Dolg, M.; Stoll, H.; Preuss, H. *Theor. Chim. Acta* **1990**, *77*, 123−141.
(56) Martin, J. M. L.; Sundermann, A. *J. Chem. Phys.* **2001**, *114*, 3408.
(57) Tomasi, J.; Mennucci, B.; Cammi, R. *Chem. Rev.* **2005**, *105*, 2999−3093.
(58) van Lenthe, E.; Ehlers, A.; Baerends, E. J. *J. Chem. Phys.* **1999**, *110*, 8943−8953.
(59) Klamt, A.; Schüürmann, G. *J. Chem. Soc., Perkin Trans. 2* **1993**, 799−805.
(60) Wang, F.; Ziegler, T.; van Lenthe, E.; van Gisbergen, S.; Baerends, E. J. *J. Chem. Phys.* **2005**, *122*, 204103.
(61) Wang, F.; Ziegler, T. *J. Chem. Phys.* **2005**, *123*, 154102.
(62) Dattelbaum, D. M.; Omberg, K. M.; Schoonover, J. R.; Martin, R. L.; Meyer, T. J. *Inorg. Chem.* **2002**, *41*, 6071−6079.
(63) Asbury, J. B.; Wang, Y.; Lian, T. *Bull. Chem. Soc. Jpn.* **2002**, *75*, 973−983.
(64) Liard, D. J.; Busby, M.; Matousek, P.; Towrie, M.; Vlček, A., Jr. *J. Phys. Chem. A* **2004**, *108*, 2363−2369.
(65) Gabrielsson, A.; Matousek, P.; Towrie, M.; Hartl, F.; Záliš, S.; Vlček, A., Jr. *J. Phys. Chem. A* **2005**, *109*, 6147−6153.
(66) Franco, C.; Olmsted, J., III. *Talanta* **1990**, *37*, 905−909.
(67) Rossenaar, B. D.; George, M. W.; Johnson, F. P. A.; Stufkens, D. J.; Turner, J. J.; Vlček, A., Jr. *J. Am. Chem. Soc.* **1995**, *117*, 11582−11583.
(68) Gabrielsson, A.; Busby, M.; Matousek, P.; Towrie, M.; Hevia, E.; Cuesta, L.; Perez, J.; Záliš, S.; Vlček, A., Jr. *Inorg. Chem.* **2006**, *45*, 9789−9797.
(69) Gabrielsson, A.; Hartl, F.; Zhang, H.; Lindsay Smith, J. R.; Towrie, M.; Vlček, A., Jr.; Perutz, R. N. *J. Am. Chem. Soc.* **2006**, *128*, 4253−4266.
(70) Stufkens, D. J.; Aarnts, M. P.; Rossenaar, B. D.; Vlček, A., Jr. *Pure Appl. Chem.* **1997**, *69*, 831−835.
(71) Worl, L. A.; Duesing, R.; Chen, P.; Della Ciana, L.; Meyer, T. J. *J. Chem. Soc., Dalton Trans.* **1991**, 849−858.
(72) Miki, H.; Shimada, M.; Azumi, T.; Brozik, J. A.; Crosby, G. A. *J. Phys. Chem.* **1993**, *97*, 11175−11179.
(73) Komada, Y.; Yamauchi, S.; Hirota, N. *J. Phys. Chem.* **1986**, *90*, 6425−6430.
(74) Finkenzeller, W. J.; Stößel, P.; Yersin, H. *Chem. Phys. Lett.* **2004**, *397*, 289−295.
(75) Striplin, D. R.; Crosby, G. A. *Chem. Phys. Lett.* **1994**, *221*, 426−430.
(76) Blanco-Rodríguez, A. M.; Towrie, M.; Clark, I. P.; Záliš, S.; Vlček, A., Jr. *Manuscript in preparation*.
(77) Blanco-Rodríguez, A. M.; Towrie, M.; Collin, J.-P.; Záliš, S.; Vlček, A., Jr. *Dalton Trans.* **2009**, 3941−3949.
(78) Turro, N. J.; Scaiano, J. C.; Ramamurthy, V. *Modern Molecular Photochemistry of Organic Molecules*; University Science Book: Sausalito, CA, 2010.
(79) Pomestchenko, I. E.; Castellano, F. N. *J. Phys. Chem. A* **2004**, *108*, 3485−3492.
(80) Danilov, E. O.; Pomestchenko, I. E.; Kinayyigit, S.; Gentili, P. L.; Hissler, M.; Ziessel, R.; Castellano, F. N. *J. Phys. Chem. A* **2005**, *109*, 2465−2471.
(81) Danilov, E. O.; Rachford, A. A.; Goeb, S.; Castellano, F. N. *J. Phys. Chem. A* **2009**, *113*, 5763−5768.
(82) Prusakova, V.; McCusker, C. E.; Castellano, F. N. *Inorg. Chem.* **2012**, *51*, 8589−8598.
(83) Haskins-Glusac, K.; Ghiviriga, I.; Abboud, K. A.; Schanze, K. S. *J. Phys. Chem. B* **2004**, *108*, 4969−4978.
(84) Alberding, B. G.; Chisholm, M. H.; Gallucci, J. C.; Ghosh, Y.; Gustafson, T. L. *Proc. Natl. Acad. Sci. U.S.A.* **2011**, *108*, 8152−8156.
(85) Chisholm, M. H.; Gustafson, T. L.; Turro, C. *Acc. Chem. Res.* **2012**, *46*, 529−538.
(86) Steffen, A.; Tay, M. G.; Batsanov, A. S.; Howard, J. A. K.; Beeby, A.; Vuong, K. Q.; Sun, X.-Z.; George, M. W.; Marder, T. B. *Angew. Chem., Int. Ed.* **2010**, *49*, 2349−2353.
(87) Siddique, Z. A.; Yamamoto, Y.; Ohno, T.; Nozaki, K. *Inorg. Chem.* **2003**, *42*, 6366−6378.
(88) Siddique, Z. A.; Ohno, T.; Nozaki, K. *Inorg. Chem.* **2004**, *43*, 663−673.

(89) Durrell, A. C.; Keller, G. E.; Lam, Y.-C.; Sýkora, J.; Vlček, A., Jr.; Gray, H. B. *J. Am. Chem. Soc.* **2012**, *134*, 14201−14207.
(90) Yersin, H. *Transition Metal and Rare Earth Compounds*; Topics in Current Chemistry; Springer: New York, 2004; Vol. *241*, pp 1−26.
(91) Yersin, H.; Finkenzeller, W. J. In *Highly Efficient OLEDs with Phosphorescent Materials*; Yersin, H., Ed.; Wiley-VCH: Weinheim, 2008; pp 1−97.
(92) Rausch, A. F.; Homeier, H. H. H.; Yersin, H. *Top. Organomet. Chem.* **2010**, *29*, 193−235.
(93) Yersin, H.; Rausch, A. F.; Czerwieniec, R.; Hofbeck, T.; Fischer, T. *Coord. Chem. Rev.* **2011**, *255*, 2622−2652.
(94) Smith, M. B.; Michl, J. *Chem. Rev.* **2010**, *110*, 6891−6936.